ELSEVIER

Journal of Structural Geology 26 (2004) 491–501

JOURNAL OF STRUCTURAL GEOLOGY

www.elsevier.com/locate/jsg

Geometry and kinematic evolution of Riedel shear structures, Capitol Reef National Park, Utah

Yoram Katz[a,b,*], Ram Weinberger[b], Atilla Aydin[c]

[a]*Institute of Earth Sciences, Hebrew University of Jerusalem, Jerusalem 95501, Israel*
[b]*Geological Survey of Israel, Jerusalem, Israel*
[c]*Department of Geological and Environmental Sciences, Stanford University, Stanford, CA, USA*

Received 27 November 2002

Abstract

Riedel shear structures are common fault patterns identified within shear zones and related to the embryonic stages of fault formation. This study focuses on the geometry of outcrop-scale natural shear zones consisting of different generations of Riedel structures, exposed in the Jurassic Navajo sandstone, Capitol Reef National Park, Utah. Geometric analysis of different structures shows that the spacing of synthetic R-deformation bands increases with the spacing of antithetic R′-deformation bands. Systematic correlation is found between the R-band spacing and the angles formed between R- and R′-bands. Examination of young Riedel structures shows their tendency to localize along narrow, elongated domains sub-parallel to the shear direction and create denser Riedel networks. We suggest that the evolution of Riedel structures is dominated by two mechanisms: (1) discrete faulting in the form of conjugate deformation bands, generally complying with the Mohr–Coulomb criteria, and (2) granular flow, which rotates mainly the R′-deformation bands. Both mechanisms are intensified with progressive strain, decreasing the deformation-band spacing and increasing the R- to R′-angles. The tendency of young Riedel structures to organize in dense elongated networks is related to strain localization during the shear-zone evolution. We suggest a kinematic explanation for the evolution of Riedel-structure networks, which relates the network geometry to the progressive accumulation and localization of shear strain.

Keywords: Deformation bands; Riedel structures; Strain localization; Shear zones

1. Introduction

Riedel structures are networks of shear bands, commonly developed in zones of simple shear during the early stages of faulting. The basic geometry of the Riedel structure consists of conjugate shear bands arranged in en-échelon arrays and denoted by R and R′ (Fig. 1). The R- and R′-bands create an angle of about $\phi/2$ and $90 - \phi/2$ to the general shear-zone direction, respectively, and intersect in an acute angle of $\beta = 90 - \phi$, where ϕ is the angle of internal friction (Riedel, 1929; Tchalenko, 1968). The R-bands are synthetic to the sense of slip across the shear-zone, forming right-stepping en-échelon arrays along sinistral shear-zones and left-stepping arrays along dextral shear-zones. The R′-bands are antithetic, and usually connect overlapping R-bands. The Riedel shear structure, first reported by Cloos (1928) and Riedel (1929) in clay-cake experiments, was realized to be a fundamental structure within shear-zones. Studies of macro-scale fault systems have associated these structures with strike-slip displacement induced by earthquakes (Tchalenko, 1970), basement faulting (Moore, 1979) and interplate shearing (Cunningham, 1993). Studies in meso-scale (e.g. Jamison and Stearns, 1982; Antonellini and Aydin, 1995; Davis et al., 1999; Ortlepp, 2000; Ahlgren, 2001), micro-scale (e.g. Jamison and Stearns, 1982; Arboleya and Engelder, 1995) and laboratory experiments (e.g. Tchalenko, 1970; Naylor et al., 1986) documented Riedel structures of various sizes within different rock types and geologic settings.

The present study focuses on the geometrical characterization and time relationship between Riedel shear structures within the Jurassic Navajo sandstone in Capitol Reef National Park, Utah (Fig. 2). The cataclastic shear bands

* Corresponding author. Tel.: +972-2-5314211; fax: +972-2-5380688.
E-mail address: k_yoram@mail.gsi.gov.il (Y. Katz).

0191-8141/$ - see front matter © 2003 Elsevier Ltd. All rights reserved.
doi:10.1016/j.jsg.2003.08.003

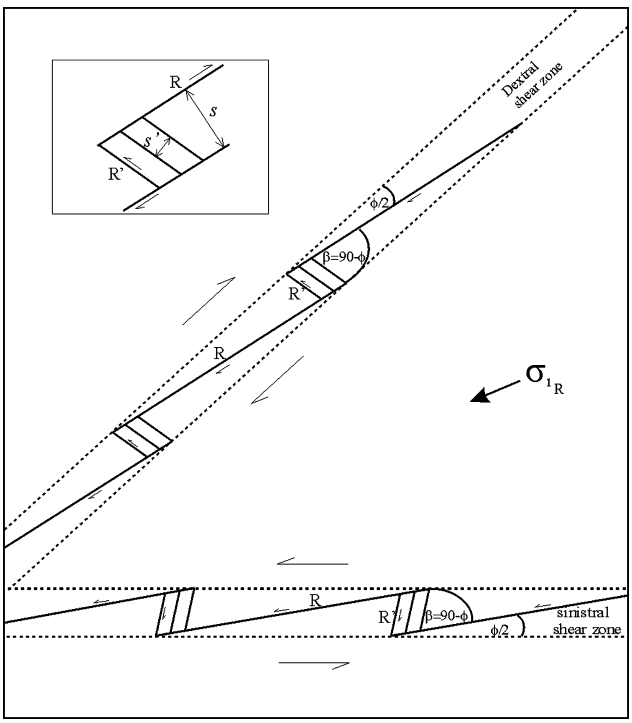

Fig. 1. Basic Riedel shear structures forming sinistral and dextral conjugate shear-zones. R and R′ are synthetic and antithetic shear bands, β is the angle between R and R′ and ϕ is the angle of internal friction. σ_{1R} denotes the remote maximum compressive principal stress. Inset: definition of s (R-band spacing) and s' (R′-band spacing).

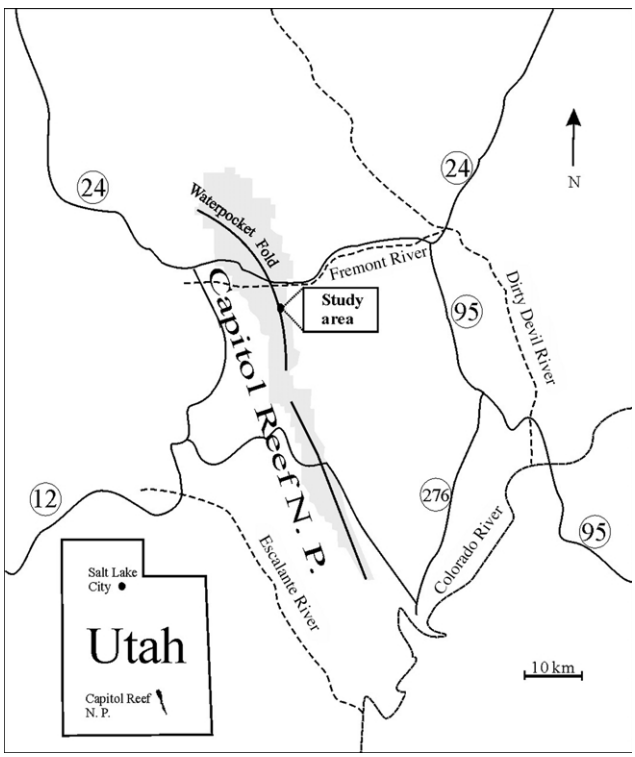

Fig. 2. Location map of Capitol Reef National Park and the study area. Highways and their numbers are indicated.

forming Riedel structures in sandstone, commonly termed deformation bands, are typically ~1 mm in width and may have offsets of several millimeters. Their formation is associated with collapse of pore space, breakage and crushing of grains, and a major reduction of porosity and permeability (Aydin, 1978; Aydin and Johnson, 1978; Antonellini and Aydin, 1994). Analysis of dozens of discrete and nested Riedel structures has shown systematic correlation between the geometry, the distribution and the relative age of the structures. This correlation may have significant implications with regard to the prediction of shear zone architecture during accumulation of strain. Moreover, knowing the average permeability of a single deformation band and once the shear zone architecture is well defined, hydrological variables of the fault zone, as conductivity tensor, bulk porosity and tortuosity can be evaluated. Motivated by the major structural and hydrological significance, this study suggests a kinematic model for the development of Riedel-structure networks and correlates them with progressive deformation within shear zones.

2. Geological setting

The study area is located along the Waterpocket monocline in Capitol Reef National Park, where Riedel shear structures are well exposed within outcrops of the Jurassic Navajo sandstone. Data was collected at the northern bank of Capitol Wash, which crosses the monocline from west to east, 6 km south of the Fremont River (Fig. 2). The NW–N-trending monocline is believed to have initiated at ~75 Ma and to have ceased activity prior to the Eocene (Baker, 1935; Kelley, 1955; Dumitru et al., 1994). The Navajo Formation consists of porous, quartz-rich sandstone and exhibits whitish, cross-bedded massive outcrops (Kiersch, 1950; Marzolf, 1983, 1990; Antonellini and Aydin, 1994). It is underlain by shales and sandstones of the Jurassic Glen–Canyon Group and overlain by shales and sandstones of the Jurassic San Rafael Group.

Being readily deformable, the Navajo Formation exhibits various internal deformation features (e.g. Shipton and Cowie, 2001; Davatzes et al., 2003). Davis (1999) and Davis et al. (1999) carried out a structural analysis of deformation band shear-zones in south-central Utah, including the north-central and southern parts of the Waterpocket monocline. In the Sheets Gulch area, located approximately 16 km south of the present study area, strike-slip shear-zones consisting of Riedel structures were reported to occur in two conjugate sets, a dextral set striking NE, and a sinistral set striking ESE, both showing high dip angles of ~75°. Davis et al. (1999) suggested that the conjugate sets accommodated strain during the Laramide regional shortening perpendicular to the Waterpocket monocline hinge, and Roznovsky and Aydin (2001) proposed that major Riedel-structure networks concentrate in areas where the monocline changes its

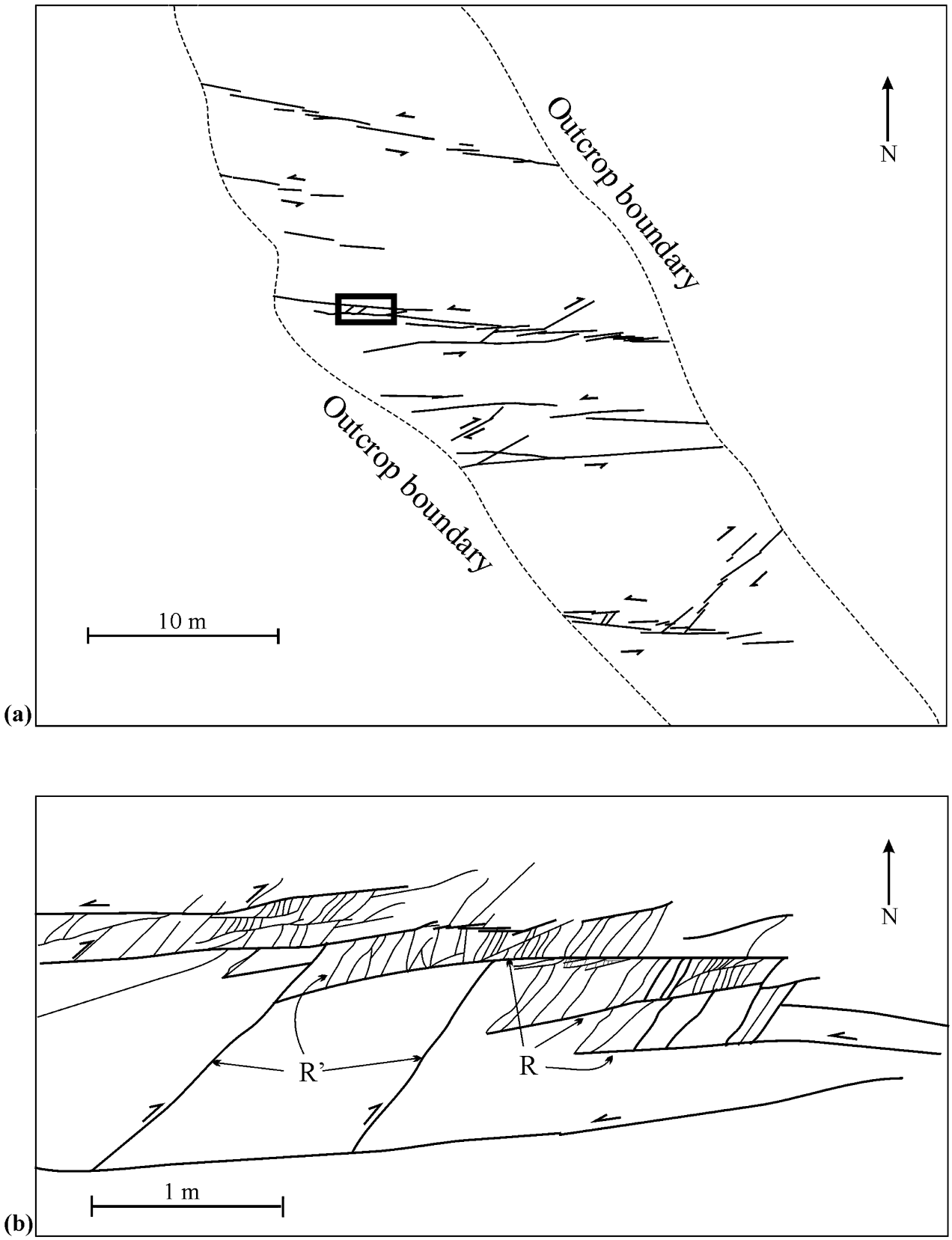

Fig. 3. (a) Conjugate sets of E-trending sinistral and NE-trending dextral shear-zones. The rectangle marks the location of the detailed map in (b). (b) R-deformation bands arranged in en-échelon, right-stepping manner within an E-trending sinistral shear-zone. Overlapping R-bands are connected by NE-trending dextral R′ arrays and form nested Riedel structures of different sizes.

orientation due, perhaps, to underlying fault geometry. Ahlgren (2001) showed systematic spatial change in the geometry of the shear-bands at Sheets Gulch. He identified gradual stages of complexity of the Riedel structures along shear zones and associated them with increasing strain accommodation. Based on fission-track data, Dumitru et al. (1994) constrained the maximum temperature and burial depth of Permian Waterpocket rocks to be ~85–95 °C and 2–3 km just before the creation of the monocline. Assuming a normal geothermal gradient, this implies a maximum temperature and burial depth of ~60 °C and 1–2 km for the overlain Navajo sandstone at that time.

3. Field observations

Documentation of the Riedel networks in Capitol Wash was carried out using electronic distance measurement (EDM) for medium scales, digital hand photography for small scales and compass and tape for direct measurements of orientations, spacing and displacements. The E-trending (090° ± 10°) zones exhibit horizontal striae with sinistral offsets, and consist of synthetic, right-stepping en-échelon R-deformation bands (Fig. 3a). The NE-trending (045° ± 10°) zones exhibit horizontal striae with dextral offsets, and consist of synthetic, left-stepping en-échelon R-deformation bands. Commonly, the R-deformation bands in the E- and NE-trending zones are connected by antithetic R′-deformation bands, both of which form Riedel networks in conjugate sets (Fig. 3b).

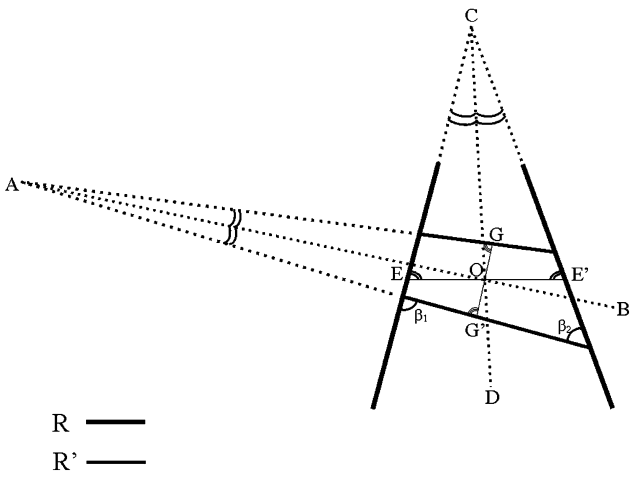

Fig. 4. Geometrical definitions of R-band spacing (s), R′-band spacing (s') and the R to R′ angle (β). The R-bands and each pair of adjacent R′-bands define a parallelogram, centered by the intersection of two lines: A–B, which bisects the angle between the R′-bands, and C–D, which bisects the angle between the R-bands. The R-band spacing (E–E′) within this parallelogram is defined as the length of the line connecting the R-bands, creating identical angles with them and passing through the parallelogram center O. Similarly, the R′-band spacing (G–G′) is defined as the length of the line connecting the R′-bands, creating identical angles with them and passing through O. The angle β is evaluated as the average of the two alternating angles, created between the R′-band and the confining R-bands (β_1 and β_2).

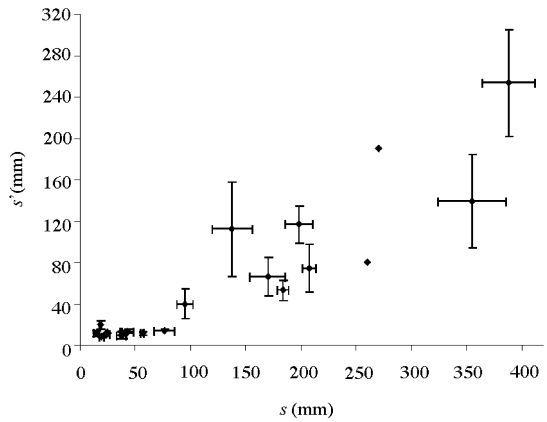

Fig. 5. Relationship between the R′-band spacing (s') and the bounding R-band spacing (s) within Riedel structures of different sizes, showing a general increase of s' with s. As the bands are not strictly parallel, spacing was measured in more than one parallelogram within most of the structures. The rectangles represent the average values for a given structure and the bars demonstrate two standard deviations.

In order to geometrically characterize the Riedel shear structures and understand their evolution, structures of different sizes were analyzed by measuring the R-band spacing (denoted s), R′-band spacing (denoted s') and the angle between R and R′-bands (denoted β) (Fig. 1). As the bands are not strictly parallel, spacing and angles were measured using the technique presented in Fig. 4. The geometrical analysis revealed the following:

1. A plot of R′-band spacing (s') versus R-band spacing (s), showing a general increase of s' with s (Fig. 5).

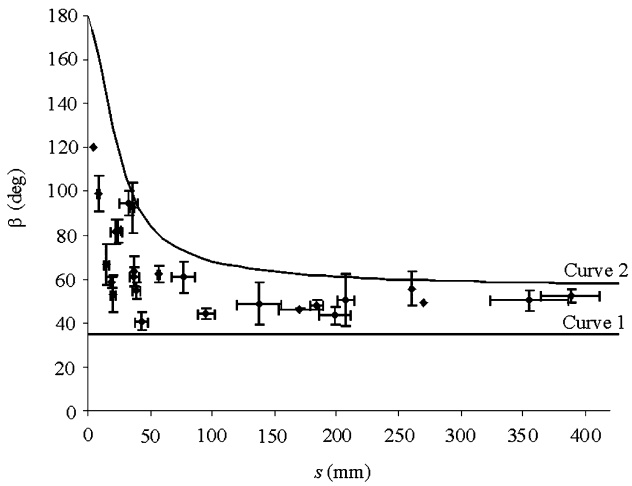

Fig. 6. Relationship between the R-band spacing (s) and the R to R′ angle (β). Spacing and angles were measured in more than one parallelogram within most of the structures. The rectangles represent the average values and the bars demonstrate two standard deviations. Noticeably, most Riedel structures of R spacing greater than ~80 mm tend to form β values of $35° < \beta < 60°$, whereas structures of smaller R spacing exhibit a variety of angles that may reach 120°. Curves 1 and 2 were calculated by the proposed kinematic model and predict the minimum and maximum β values expected for a given s, respectively (see details in Section 4).

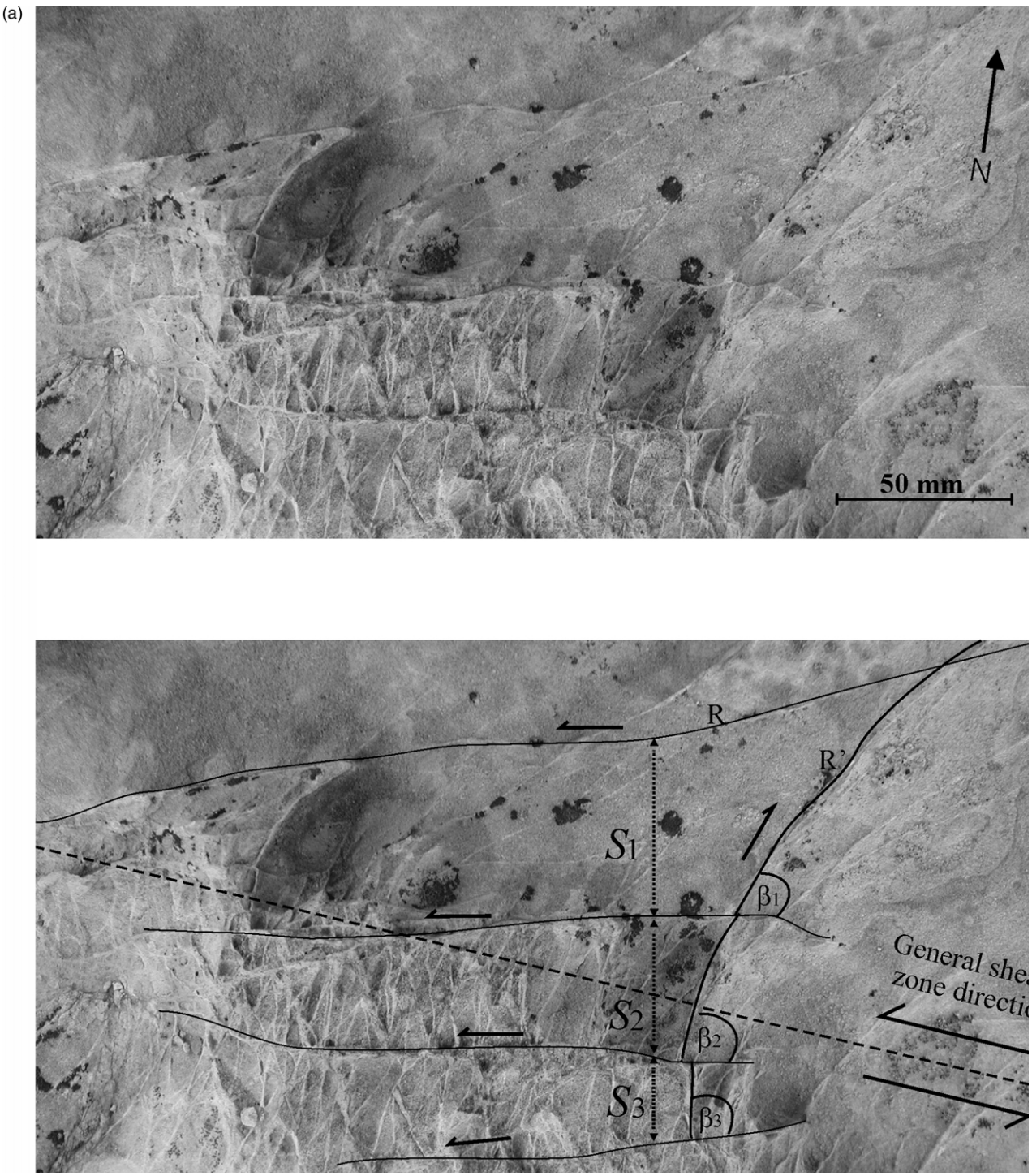

Fig. 7. (a) Riedel shear structures within E-trending sinistral shear-zone. Representative major deformation bands demonstrate the increase of β with decrease of s. R′ band (thick line) intersects adjacent sinistral R-bands (thin lines), creating β angles of 60, 75 and 85° (β_1, β_2 and β_3, respectively) as s values are 52, 38 and 24 mm (s_1, s_2 and s_3, respectively). (b) Riedel shear structures within NE-trending dextral shear-zone. The orientation of the sinistral R′ band (thick line) is changed, resulting in β values varying from ~45° near the tip of the band (β_1) to ~90° in the interior region (β_2). Several other long, sigmoidal-like shaped R′-bands extend beyond the domains bounded by the R-bands, and are clearly offset by the R-bands. These R′-bands were recognized by Ahlgren (2001) to be the first structural elements created during early stages of the shear zone evolution.

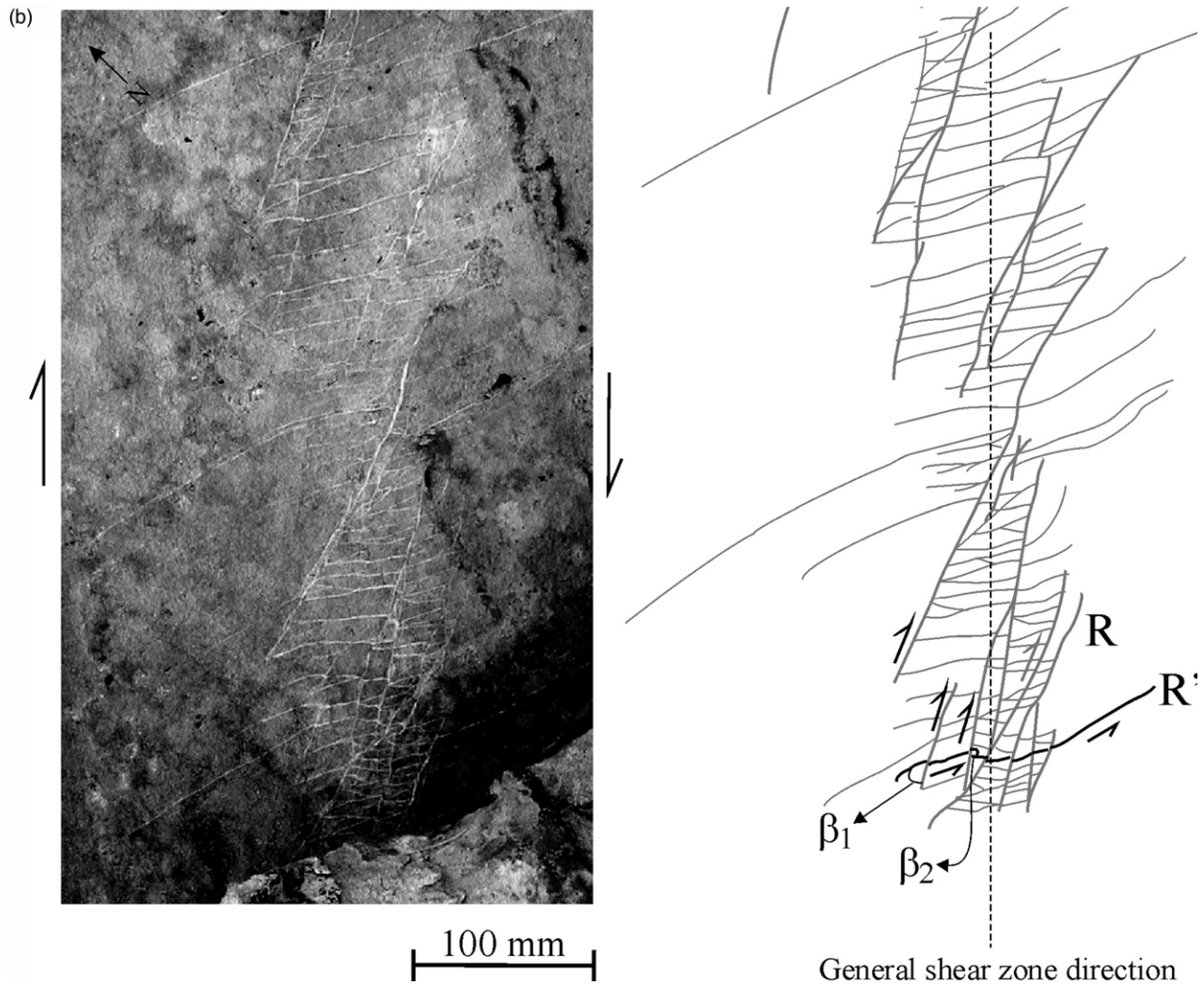

Fig. 7 (*continued*)

2. A plot of R-band spacing (s) versus the angle between R- and R′-bands (β), showing a systematic relationship between s and β (Fig. 6). Generally, Riedel structures exhibiting values of $s > 80$ mm form angles of $35° < \beta < 60°$. Structures of $s \leq 80$ mm form a larger range of angles, $35° < \beta < 100°$, and in rare cases the angle may reach 120°. The systematic relationship between s and β and the significance of their lower and upper bound values are demonstrated for an E-trending shear-zone (Fig. 7a). In this case, an R′-band is displaced by sinistral R-bands and divided into three segments. As R-band spacing s decreases, the angle β between the segment and the bounding R-bands increases such that $\beta_3 > \beta_2 > \beta_1$. Fig. 7b shows a NE-trending shear-zone, where dextral R-bands displace and divide an R′-band into several segments. The angle β varies from ~45° near the band's tips (β_1) to ~90° in the interior region of the shear-zone (β_2), where the R-bands are closely spaced, corresponding to smaller values of s. This variation results in segmented R′-bands with a general trace geometry that resembles a sigmoidal-like shape.
3. Detailed examination of several shear zones reveals a relationship between the relative age of the Riedel structure and the angle between R- and R′-bands, β. Commonly, young Riedel structures overprint old structures within the shear zones (Fig. 8). In these cases, the young structures exhibit smaller β angles than those of the old structures ($\beta_2 > \beta_1$ in Fig. 8).
4. Examination of nested Riedel structures reveals a systematic relationship between the relative age and the spatial extent of the structure. Old Riedel structures usually consist of widely spaced R- and R′-bands (s and s' are relatively high), and are widely distributed across the shear-zone (see Figs. 8 and 9). Young, overprinting Riedel structures exhibit a denser band framework and tend to localize along elongated domains sub-parallel to the shear direction. Fig. 9 shows a complex network of Riedel structures within a sinistral shear-zone. The primary Riedel structure is widely spaced and extends across the entire shear-zone. It is overprinted by succeeding

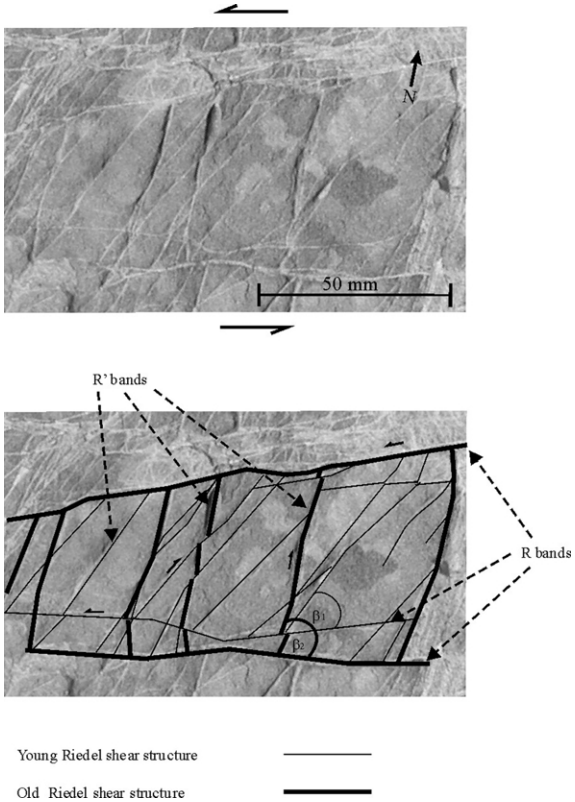

Fig. 8. Young Riedel shear structure (thin lines) overprinting an old Riedel shear structure (thick lines) within a sinistral shear-zone. The deformation bands of the young structure create a denser framework and smaller β angles (demonstrated by β_1) compared with the spacing and β angles (demonstrated by β_2) of the old structure.

secondary Riedel structures, which tend to localize into dense networks.

4. Geometrical analysis and the impact of shear strain on Riedel geometry

The field observations show a variety of Riedel structure geometries. One possibility is that the structures originally formed with different geometries due to variations in the host-rock properties, stress states, ambient temperature or pore pressure during their evolution. Alternatively, the structures might have formed according to the basic Riedel geometry and subsequently changed during progressive deformation. As slip on deformation bands is limited, new bands form during strain accommodation, and the spacing between them is reduced. In addition, grain flow sub-parallel to the R-bands, generated by the increasing stress, may rotate the R′-bands to different orientations. Assuming that different β angles measured between R- and R′-deformation bands are a consequence of rotation, the geometrical relationship between the R-spacing (s), the R to R′ angle prior to rotation (β_0) and after rotation (β), and the overall displacement over the Riedel shear structure (d) is given by (Fig. 10) (Ramsay and Huber, 1983):

$$\tan\beta = \frac{\tan\beta_0}{1 - (\tan\beta_0)\frac{d}{s}} \quad (1)$$

This can be further expressed as:

$$\frac{d}{s} = \frac{\sin(\beta - \beta_0)}{\sin\beta_0 \sin\beta} \quad (2)$$

where d/s is the shear strain across the zone, defined primarily by sub-parallel R-bands, and $(\beta - \beta_0)$ is the line rotation angle.

In order to test the above model and establish the relationship between s and β, measured values of β_0 and d were inserted into Eq. (2). β_0 was measured directly within structures showing no sign of rotation, and was found to range from 35 to 55°. This range is further supported because it also resembles the angle between the large-scale E- and NE-trending conjugate strike-slip faults (Fig. 3). According to the Anderson (1942) theory of faulting, based on the Mohr–Coulomb failure criterion, conjugate strike-slip faults intersect at an angle of $(90 - \phi)$ where ϕ is the internal friction angle of the rock ($\phi = \sim 45°$ in the present case study). As the R-bands and R′-bands within Riedel structures may also be considered as conjugate sets, it is reasonable that they were initially intersected by β_0 ranging from 35 to 55° as well. The measurements of d revealed values up to 30 mm. According to the proposed model, both β_0 and d contribute to the final angle β. Curve 1 in the s versus β data (Fig. 6) was calculated using the lowest values of the β_0 and d ranges (i.e. 35° and null displacement, respectively) and predicts the minimum β values expected for a given s. Curve 2 was calculated using the highest values of the β_0 and d ranges (55° and 30 mm, respectively) and predicts the maximum β values expected for a given s. Noticeably, most of the field measurements are incorporated between these two theoretical curves, suggesting that the proposed model is plausible.

5. Discussion

Differences in the Riedel structure geometry may occur due to dissimilarities in rock properties, such as packing, sorting, clay content and other factors governing the angle of internal friction (Underhill and Woodcock, 1987). Moore and Byerlee (1992) correlated geometrical variations to different sliding behavior of the shear-zones, where small β angles are associated with a stable slip and large β angles with stick slip. They further proposed, based on laboratory data, that larger β angles were favored by an increase in temperature and effective pore pressure. The effect of pore-fluid pressure on β values was also discussed by Gamond (1983), Dresen (1991), Byerlee (1992) and Ahlgren (2001).

In the present study, field observations demonstrate different β angles within adjacent and nested Riedel

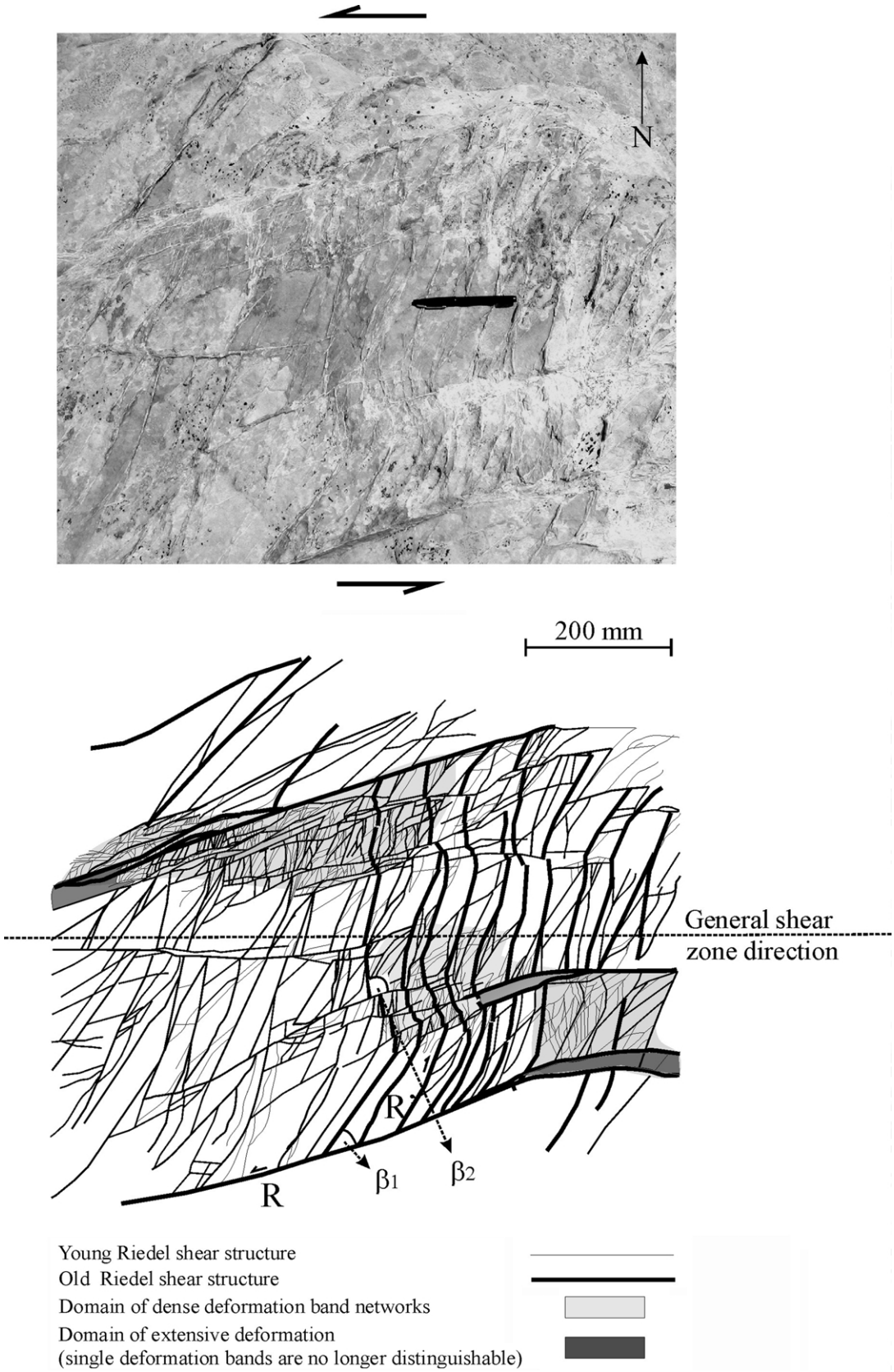

Fig. 9. Network of Riedel structures within a sinistral shear-zone. Widely-spaced, evenly distributed deformation bands forming a primary Riedel structure (thick lines) are displaced by succeeding secondary, shorter R and R′-bands, which tend to localize into dense networks. Noticeably, the primary R′-bands form an angle of ~40° with the R-bands within domains of sparse deformation (β_1). This angle is typically between 60 and 90° within the dense network domains (β_2).

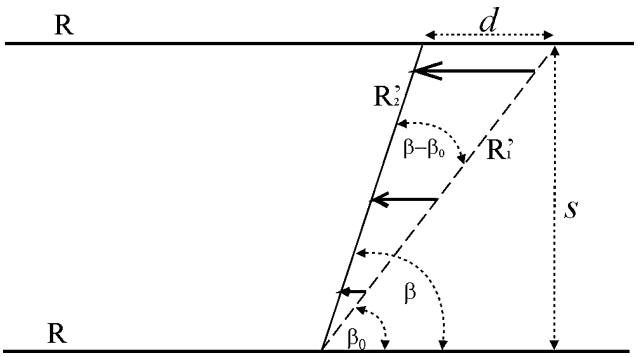

Fig. 10. Geometric relationship between the R-spacing (s), the R to R'_1 angle prior to rotation (β_0), the R to R'_2 angle after rotation (β) and the overall displacement along the shear direction (d). Dashed and solid lines represent R′-band before and after rotation, respectively. Solid arrows represent direction and magnitude of particle movement.

structures. Considering the proximity in space, and perhaps in time of the structures, it is unlikely that variations in rock properties, temperature or pore pressure provide an adequate explanation for the geometrical differences documented in the field. Alternatively, geometrical differences may be a result of rotation, either of the stress field due to local mechanical influences of the nearby propagating shear bands (Lajtai, 1969; Dresen, 1991; Shipton and Cowie, 2001), or of the shear bands themselves following their evolution (Jamison and Stearns, 1982; Mandl, 1987; Arboleya and Engelder, 1995; An and Sammis, 1996; Ahlgren, 2001). While not excluding the possibility of stress-field rotation, the present observations provide considerable evidence supporting the rotation of the shear bands themselves as material markers. We therefore propose that the deformation bands were originally oriented according to the basic Riedel structure, and later rotated during progressive deformation. As the deformation bands divide the rock into blocks, it is possible that these blocks rotated in a 'bookshelf' manner under simple shear (Mandl, 1987). This notion, however, raises three main caveats: (1) the high porosity and minor cementation of the Navajo sandstone do not favor rigid block rotation; (2) if such a rotation occurred, material gaps and overlaps should have been created along the block boundaries. Structural consequences of these phenomena are not observed in the field; (3) rotation should cause the edges of the blocks, i.e. the R and R′-bands, to rotate by the same amount. However, the field observations indicate substantial rotation of R′-bands, yet little or no rotation of R-bands within the same structures (e.g. Fig. 8).

Therefore, we propose that two coupling mechanisms are associated with progressive deformation: discrete faulting, which creates basic Riedel structures (Fig. 11a), and granular flow sub-parallel to the R-bands, which causes reorganization of the grains and rotation of the R′-deformation bands as passive markers to a new configuration (Fig. 11b). During granular flow, the elongated grains are arranged preferably sub-parallel to the shear direction

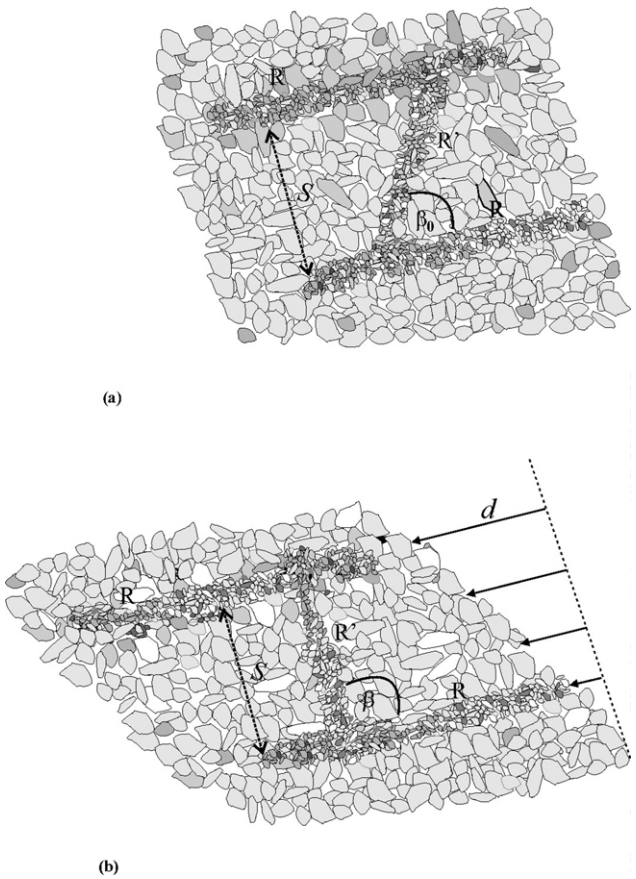

Fig. 11. Schematic presentation of Riedel-structure evolution. (a) Discrete faulting forming R and R′-deformation bands. (b) Rotation of the R′-bands due to granular flow sub-parallel to R-bands within the domain bounded by R-bands. See definitions of variables in Fig. 10.

(Cashman and Cashman, 2000). The notion of coupling discrete faulting and material flow is discussed by Borradaile (1981) and is consistent with previous work based on laboratory experiments (Tchalenko, 1970) and field data analysis (Ahlgren, 2001). In his work, Ahlgren (2001) suggested that faulting and compaction could induce locally elevated fluid pressure, which facilitates non-destructive reorganization of grains and consequent rotation of deformation bands.

The present work combines the relationships between the orientation, spacing, distribution and relative age of the deformation bands in sandstone, and provides a kinematic model for the evolution of complex networks of Riedel structures. We suggest that the observed relationship among R-band spacing and the angle between R- and R′-band (Fig. 6) reflects the coupled deformation mechanisms generated by the imposed strain, as follows:

1. With progressive deformation, discrete faulting creates denser Riedel networks. The faulting affects both the R-band and the R′-band spacing (Fig. 12a and b), as reflected in the monotonous relationship between s and s' (Fig. 5). Likewise, Jamison and Stearns (1982),

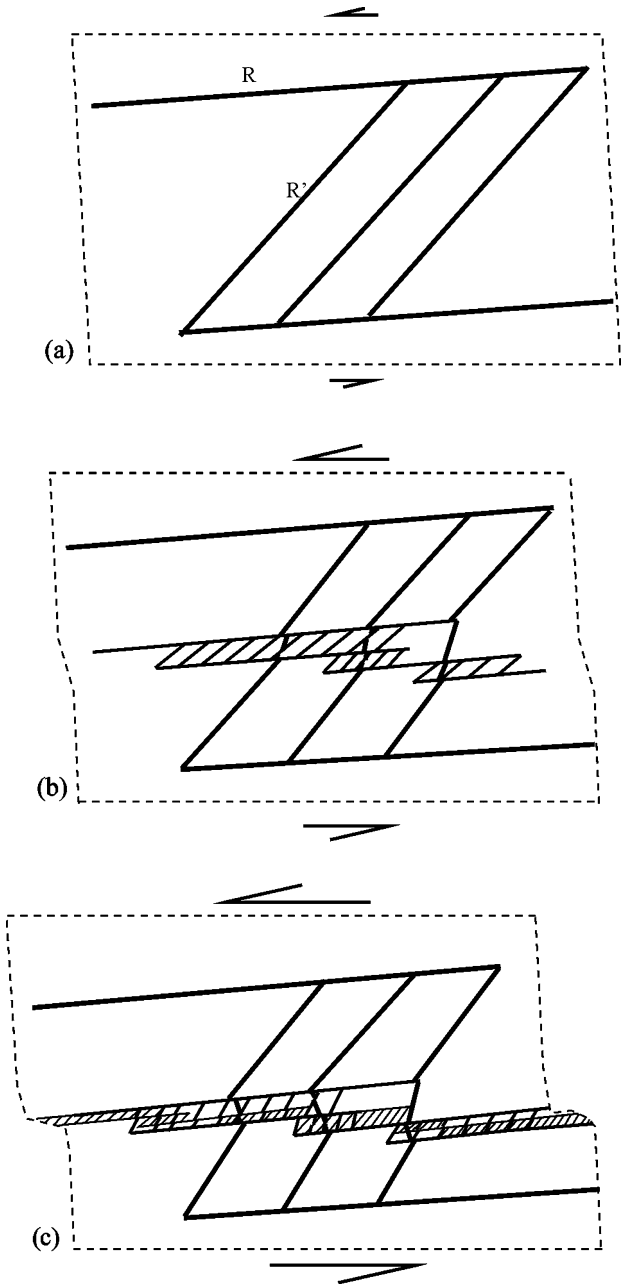

Fig. 12. Stages in the evolution of complex Riedel shear structures. (a) Primary basic Riedel structure consisting of sparse, broadly distributed deformation bands is created during the first stages of shear-zone evolution. (b) With progressive strain, new closely-spaced deformation bands displace old deformation bands. (c) Dense networks of deformation bands, restricted to narrow elongated domains orienting sub-parallel to shear direction, are created at later stages of the shear-zone evolution. Due to intensive rotation within these domains the primary R′-bands change into a sigmoidal-like shape.

Antonellini and Aydin (1995) and Mair et al. (2000) reported a positive correlation between deformation-band density and imposed strain. As shown in Fig. 5, values of s' which correspond to values of $s < \sim 80$ mm tend to stabilize and average ~ 10 mm. This phenomenon may imply scaling of spacing with the average grain size, and needs further research.

2. In addition to faulting, increased granular flow excessively rotates the R′-deformation bands and reorients them according to the geometrical relationship presented in Eqs. (1) and (2) (Fig. 12b and c). Hence, Riedel structures consisting of closely spaced and highly rotated deformation bands represent domains in which incremental strain was localized within the shear-zone.

Comparison between Riedel structures of different geometries shows that dense, nested structures are restricted to narrow, elongated domains oriented sub-parallel to the general shear direction (Fig. 12c), whereas widely spaced Riedel structures are broadly distributed across the shear-zone. Field relationships further show that the dense structures are usually younger than the widely spaced structures. We therefore conclude that the variations in the density and orientation of the Riedel structural elements reflect different stages in the shear-zone evolution, as a function of the magnitude and localization of the shear strain.

6. Summary

Riedel structures are fundamental features within shear-zone architectures, and are related to early stages of the shear-zone evolution. Their development within the Navajo sandstone in the Capitol Reef National Park, Utah, is dominated by two mechanisms—discrete faulting with conjugate geometry corresponding to the Coulomb–Mohr criteria, and granular flow sub-parallel to the prominent R-deformation band direction. Different Riedel geometries reflect different degrees of shear strain; as strain accumulates, discrete faulting intensifies and the spacing between the deformation bands decreases. Granular flow across domains bounded by R-bands facilitates rotation and thereby increases the angle β between intersecting R- and R′-shear bands. Upon further strain localization, new Riedel structures are formed, offsetting and overprinting the older structures. The new structures consist of denser networks of deformation bands than those of the old Riedel structures, and are restricted to narrower and more elongated domains, sub-parallel to the general shear direction. Within these domains substantial rotation occurs, changing the primary R′-bands into a sigmoidal-like shape. This study relates the geometry of Riedel networks to accumulation and localization of shear strain, enabling better understanding of the embryonic stages of fault formation and evolution of shear-zone architectures.

Acknowledgements

We benefited from fruitful discussions with Vladimir Lyakhovsky and Avraham Starinsky. We wish to thank Eric Flodin for helpful advice concerning the fieldwork. Dave

Dewhurst, Susan Hippler and the Associated Editor, Don Fisher, provided constructive and useful reviews of the manuscript. We also thank Bevie Katz for language editing. This study was supported by grant No. 9800198 from the United States–Israel Binational Science Foundation (BSF), Jerusalem, Israel.

References

Ahlgren, S.G., 2001. The nucleation and evolution of Riedel shear-zones as deformation bands in porous sandstone. Journal of Structural Geology 23, 1203–1214.

An, L.-J., Sammis, C.G., 1996. Development of strike-slip faults: shear experiments in granular materials and clay using a new technique. Journal of Structural Geology 18, 1061–1077.

Anderson, E.M., 1942. The Dynamics of Faulting, 1st ed, Oliver and Boyd, Edinburgh.

Antonellini, M.A., Aydin, A., 1994. Effects of faulting on fluid flow in porous sandstones: petrophysical properties. American Association of Petroleum Geologists Bulletin 78, 355–377.

Antonellini, M.A., Aydin, A., 1995. Effects of faulting on fluid flow in porous sandstones: geometry and spatial distribution. American Association of Petroleum Geologists Bulletin 79, 642–671.

Arboleya, M.L., Engelder, T., 1995. Concentrated slip zones with subsidiary shears: their development on three scales in the Cerro Brass fault zone, Appalachian valley and ridge. Journal of Structural Geology 17, 519–532.

Aydin, A., 1978. Small faults formed as deformation bands in sandstones. Pure and Applied Geophysics 116, 913–930.

Aydin, A., Johnson, A.M., 1978. Development of faults as zones of deformation bands and as slip surfaces in sandstone. Pure and Applied Geophysics 116, 931–942.

Baker, A.A., 1935. Geologic structure of southeastern Utah. American Association of Petroleum Geologists Bulletin 19, 1472–1507.

Borradaile, G.J., 1981. Particulate flow of rock and formation of cleavage. Tectonophysics 72, 305–321.

Byerlee, J., 1992. The change in orientation of subsidiary shears near faults containing pore fluid under high pressure. Tectonophysics 211, 295–303.

Cashman, S., Cashman, C., 2000. Cataclasis and deformation-band formation in unconsolidated marine terrace sand, Humboldt County, California. Geology 28, 111–114.

Cloos, H., 1928. Experimenten zur inneren Tektonic. Centralblatt fur Mineralogie und Paleontologie B, 609.

Cunningham, W.D., 1993. Strike-slip faults in the southernmost Andes and the development of Patagonian orocline. Tectonics 12, 169–186.

Davatzes, N.C., Aydin, A., Eichhubl, P., 2003. Overprinting faulting mechanisms during the development of multiple fault sets in sandstone, Chimney Rock fault array, Utah, USA. Tectonophysics 363, 1–18.

Davis, G.H., 1999. Structural geology of the Colorado Plateau region of southern Utah, with special emphasis on deformation bands. Geological Society of America Special Paper 342, 157pp.

Davis, G.H., Bump, A.P., Garcia, P.E., Ahlgren, S.G., 1999. Conjugate Riedel deformation band shear-zones. Journal of Structural Geology 22, 169–190.

Dresen, G., 1991. Stress distribution and the orientation of Riedel shears. Tectonophysics 188, 239–247.

Dumitru, T.A., Duddy, I.A., Green, P.F., 1994. Mesozoic–Cenozoic burial, uplift and erosion history of the west-central Colorado Plateau. Geology 22, 499–502.

Gamond, J.F., 1983. Displacement features associated with fault zones: a comparison between observed examples and experimental models. Journal of Structural Geology 5, 33–45.

Jamison, W.R., Stearns, D.W., 1982. Tectonic deformation of Wingate sandstone, Colorado National Monument. American Association of Petroleum Geologists Bulletin 66, 2584–2608.

Kelley, V.C., 1955. Monoclines of the Colorado Plateau. Geological Society of America Bulletin 66, 789–803.

Kiersch, G.A., 1950. Small-scale structures and other features of Navajo Sandstone, northern part of the San-Rafael Swell, Utah. American Association of Petroleum Geologists Bulletin 34, 923–942.

Lajtai, E.Z., 1969. Mechanics of second order faults and tension gashes. Geological Society of America Bulletin 80, 2253–2272.

Mair, K., Main, I., Elphick, S., 2000. Sequential growth of deformation bands in the laboratory. Journal of Structural Geology 22, 25–42.

Mandl, G., 1987. Tectonic deformation by rotating parallel faults: the "bookshelf" mechanism. Tectonophysics 141, 277–316.

Marzolf, J.E., 1983. Changing winds and hydraulic regimes during deposition of the Navajo and Aztec sandstones, Jurassic(?) south-western United States. In: Brookfield, M.E., Ahlbrandt, T.S. (Eds.), Eolian Sediments and Processes, Elsevier, Amsterdam, pp. 635–660.

Marzolf, J.E., 1990. Reconstruction of extensionally dismembered early Mesozoic sedimentary basins; southwestern Colorado Plateau to the eastern Mojave Desert. In: Wernicke, B.P. (Eds.), Basin and Range Extensional Tectonics near the Latitude of Las Vegas, Nevada. Geological Society of America Memior 176, pp. 477–500.

Moore, D.E., Byerlee, J., 1992. Relationship between sliding behavior and internal geometry of laboratory fault zones and some creeping and locked strike-slip faults of California. Tectonophysics 211, 305–316.

Moore, J.M., 1979. Tectonics of the Najad transcurrent fault system, Saudi Arabia. Journal of Geological Society of London 136, 441–452.

Naylor, M.A., Mandl, G., Sijpesteijn, C.H.K., 1986. Fault geometries in basement-induced wrench faulting under different initial stress states. Journal of Structural Geology 8, 737–752.

Ortlepp, W.D., 2000. Observation of mining-induced faults in an intact rock mass at depth. International Journal of Rock Mechanics and Mining Sciences 37, 423–436.

Ramsay, J.G., Huber, M.I., 1983. The Techniques of Modern Structural Geology. Volume 1: Strain Analysis, Academic Press, London.

Riedel, W., 1929. Zur Mechanik Geologischer Brucherscheinungen. Zentral-blatt fur Mineralogie, Geologie und Paleontologie B, 354–368.

Roznovsky, T.A., Aydin, A., 2001. Concentration of shearing deformation related to changes in strike of monoclinal fold axes: the Waterpocket monocline, Utah. Journal of Structural Geology 23, 1567–1579.

Shipton, Z.K., Cowie, P.A., 2001. Damage zone and slip-surface evolution over μm to km scales in high-porosity Navajo sandstone, Utah. Journal of Structural Geology 23, 1825–1844.

Tchalenko, J.S., 1968. The evolution of kink-bands and the development of compression textures in sheared clays. Tectonophysics 6, 159–174.

Tchalenko, J.S., 1970. Similarities between shear-zones of different magnitudes. Geological Society of America Bulletin 81, 1625–1640.

Underhill, J.R., Woodcock, N.H., 1987. Faulting mechanism in high-porosity sandstones; New Red Sandstone, Arran, Scotland. In: Jones, M.E., Prestone, R.M.F. (Eds.), Deformation of Sediments and Sedimentary Rocks. Geological Society of London Special Publication, 29, pp. 91–105.